Research papers

Assessing precipitation from a dual-polarisation X-band radar campaign using the Grid-to-Grid hydrological model

John R. Wallbank [a],[*], David Dufton [b], Ryan R. Neely III [b],[c], Lindsay Bennett [b],[c], Steven J. Cole [a], Robert J. Moore [a]

[a] UK Centre for Ecology & Hydrology, Wallingford OX10 8BB, UK
[b] National Centre for Atmospheric Science, Leeds, UK
[c] School of Earth and Environment, University of Leeds, Leeds, UK

ARTICLE INFO

ABSTRACT

A set of Quantitative Precipitation Estimates (QPEs) from a dual-polarisation X-band radar observation campaign in a mountainous area of Northern Scotland is assessed with reference to observed river flows as well as being compared to estimates from the UK C-band radar and raingauge networks. Employing estimation methods of varying complexity, the X-band QPEs are trialled as alternative inputs to Grid-to-Grid (G2G), a distributed hydrological model, to produce simulated river flows for comparison with observations. This hydrological assessment complements and extends a previous meteorological assessment that used point raingauge data only. Precipitation estimates for two periods over the observation campaign in 2016 (March to April and June to August) are assessed. During the second period, increased incorporation of dual-polarisation variables into the radar processing chain is found to be of considerable benefit, whereas during the first period the low height of the melting layer often restricts their use. As a result of the complex topography in Northern Scotland, the Lowest Usable Elevation (LUE) of the X-band radar observations is found to be a stronger indicator of the hydrological model performance than range from the radar. For catchments with an LUE of less than 3 km, the best X-band QPE typically performs better for modelling river flow than using an estimate from the UK C-band radar network. The hydrological assessment framework used here brings fresh insights into the performance of the different QPEs, as well as providing a stimulus for targeted improvements to dual-polarisation radar-based QPEs that have wider relevance beyond the case study situation.

1. Introduction

Observing, in a quantitative and robust way, the dynamic space–time pattern of precipitation in hilly and mountainous terrain presents a major challenge of great practical importance across the world. A common approach is to obtain Quantitative Precipitation Estimates (QPEs) using observations from networks of weather radars and/or raingauges. Such gridded QPEs have a wide range of applications from the images seen on weather forecasts through to their quantitative use in hydrological modelling, river flow forecasting and water resource simulation. However, there are a number of issues to be considered when forming such QPEs for high-latitude, mountainous regions.

Networks of raingauges are typically sparse in mountainous areas due to difficulties of access, so lack representativity in capturing the complex rainfall patterns found in these topographically-varied

domains. Further problems can be associated with wind-induced under-catch, solid-phase precipitation and instrument blockage, wetting and evaporation loss (Sevruk, 1982; Price, 1999). Weather radar networks provide better spatial coverage and can be used in isolation, or in combination with raingauges to make the best of these complementary sensors of areal and point rainfall. However, such radar networks often provide less than ideal observation coverage or quality in areas of high relief, due to issues such as beam blockage, range effects, and variability in the vertical profile of precipitation including changes of water phase and low-level orographic enhancement. In addition to the impact of range on beam broadening and non-uniform beam filling, overshooting of precipitation becomes more likely in areas of orography (Koistinen and Pohjola, 2014; Yu et al., 2018). A particular issue affecting high-latitude locations is the presence of a melting layer which can be close to the surface and appear as enhanced radar reflectivity via the "bright

band" effect. The robustness of radar rainfall estimates is also dependent on artefacts of the sensed environment and post-processing operations.

The introduction of dual-polarisation radar capabilities has brought benefits to precipitation estimation (Ryzhkov and Zrnić, 1995, 2019; Illingworth, 2004; Montopoli et al., 2017; Wijayarathne et al., 2020) and river flow simulation in mountainous terrain (Anagnostou et al., 2018). However, a detailed assessment of the benefits to hydrological modelling of the different dual-polarisation processing steps and retrievals has not been undertaken: this is an important novelty of the paper presented here. Studies investigating the improvement for hydrological simulation of employing dual-polarisation relative to single-polarisation are few. One example is the study by Gourley et al. (2010) for nine severe storm events from 2005 to 2008 over a 813 km^2 catchment area in Oklahoma, USA, with a hydrological focus on a 342 km^2 gauged catchment. They found that improved hydrological model performance was only achieved once long-term biases in the QPEs were identified and corrected for. Whilst the single-polarisation QPE, assessed against raingauges, had a lower bias (-9 % compared to -31 %), the best dual-polarisation QPE had a bias that was stationary whereas that of the single-polarisation QPE fluctuated with event rain-intensity, attributed to varying drop-size distributions and hail. This provides evidence for dual-polarisation stabilising the error structure across varying types of storm. Correction for bias resorted to use of the raingauge network. Seeking improvement through studies of radar QPE errors, focussed on range effects across a range of environments, was recommended for future work. A more recent hydrological assessment employing dual-polarisation radar by He et al. (2018) focussed on a flat area of Denmark with a complex hydrological regime influenced by groundwater. There was little to choose between the use of raingauge, single- and dual-polarisation QPEs for these environmental conditions, whilst the potential benefits of dual-polarisation in complex terrain was recognised.

Application of X-band dual-polarisation radars for QPE in mountainous environments has several advantages over more conventional network radars (Lim et al., 2014; Yu et al., 2018). Known limitations of X-band radar - such as their increased susceptibility to attenuation and typically lower azimuthal interval (due to smaller antenna sizes) - are less relevant in mountainous environments where topographic blockage and low-level precipitation formation typically impose severe constraints on the maximum useful radar range. The reduced cost of X-band radars - when compared to C-band or S-band systems - is particularly advantageous: making them well suited for filling gaps within existing radar networks to rectify areas of poorer local coverage. In addition, dual-polarisation has advantages in mountainous areas since phase-shift based precipitation estimators (using specific differential phase) are immune to the effects of partial beam blockage which are prevalent in such locations. This allows the use of radar observations from lower elevations than would be possible with a single polarisation system. The benefit is greatest for X-band radars as phase shift measurements from lower wavelength radars have a greater sensitivity to precipitation intensity (Sachidananda and Zrnić, 1986; Anagnostou et al., 2004).

Turning to hydrological use, based on experience limited to using networks of single-polarisation C-band radars and raingauges in the UK, precipitation estimates from raingauges have been preferred over radar-based QPEs for hydrological model development (Cole and Moore, 2008, 2009; Moore et al., 2012). Partly, this is down to the more stable error structure of raingauge data - associated with the simplicity of direct measurement and application of quality-control checks (e.g. Howard et al., 2012) - which can be partially eliminated from modelled flows during the calibration of the hydrological model.

In contrast, a range of artefacts can feature in the radar errors, arising from the sensed environment or in the post-processing, with some not readily diagnosed or corrected. Radar-based QPEs can suffer from transient under- or over-estimation of the precipitation on sub-daily and sub-hourly timescales. Although radar rainfall performance can be improved through applying radar-raingauge adjustment or merging

methods, the effect of transient errors can persist and affect estimator robustness. It is in the context of increasing QPE robustness that dual-polarisation methodologies show greatest promise for improving radar rainfall use in hydrological modelling: this is an important motivator for the work reported on here. Further, there are particular advantages in radar rainfall for hydrological applications at smaller spatial and temporal scales, such as for modelling flash-floods and in urban hydrology (Berne and Krajewski, 2013; Thorndahl et al., 2017), where convective storm cells may be missed completely by the relative sparsity of a raingauge network.

The work presented here employs a unique radar dataset from the RAiNS (Radar Applications in Northern Scotland) campaign (Bennett, 2019; Neely et al., 2021). This campaign deployed the NCAS mobile X-band dual-polarisation Doppler weather radar (NXPol), available for research studies (Neely et al., 2018), in the Scottish Highlands near Inverness over two periods in 2016. The aim of the present work is to assess the improvement to radar QPEs particularly for use as input to a hydrological model for simulating river flow over an area where the existing national network of weather radars and raingauges has known shortcomings. Importantly, it has been possible to exploit NXPol data to produce QPEs using processing chains of varying complexity and differing extent of use of dual-polarisation capability.

Previously, Neely et al. (2021) had shown that precipitation estimates from the second period of the RAiNS campaign were able to outperform estimates from the UK C-band radar network for certain parts of the study area when assessed against raingauge measurements. The present investigation aims to assess whether these benefits to QPE pass through to hydrological model simulations of river flow in mountainous locations, and ascertain any dependence on the characteristics of the catchments being modelled and the season of the year. To undertake this, NXPol-derived QPEs from both periods of the RAiNS campaign along with estimates from the UK C-band network and raingauge data are used as input to the G2G distributed hydrological model, and assessed by comparing the model-simulated river flows against observations at gauged locations. Importantly, such a hydrological assessment essentially integrates QPEs over space and time, complementing the traditional point-based meteorological comparison with raingauge data: it can provide additional insights into the performance of the QPEs, helping to stimulate future improvements to radar-based QPE methods. The hydrological approach through its space–time integration allows the radar-estimated precipitation to be evaluated over entire catchment areas, circumventing both potential raingauge issues and reducing sensitivity to localised artefacts in radar-based QPEs that may heavily influence such point-based assessments. The results of this investigation are likely to be of value to those interested in the use of dual-polarisation capabilities in networks of C-band radars, as well as for X-band radars deployed for network coverage infill purposes and for local, high-resolution applications relating to urban storm drainage management.

This paper is organised as follows. First, in Section 2, details are given of the dual-polarisation X-band radar campaign over northern Scotland including the methods of increasing complexity used in NXPol's QPE processing chain. Section 3 describes two alternative gridded QPEs included in the assessment of methods, one from the network C-band radars and the other from interpolating raingauge data. Section 4 outlines the G2G distributed hydrological model and how it is used to obtain simulated river flows from each QPE method for comparison with observations across selected catchments (detailed in Section 5). The performance statistics used to assess each QPE method, through comparison of modelled and observed river flow, are described in Section 6. Section 7 describes the performance assessment of the QPE methods and examines the influence on performance of the Lowest Usable Elevation (LUE), the radar range and the study period. A broader discussion and concluding remarks follow in Section 8.

2. The dual-polarisation X-band radar campaign over northern Scotland

2.1. Study area

The location of the NXPol radar at Kinloss Barracks, near Inverness in the Scottish Highlands, is shown as a red dot in Fig. 1a. This site was chosen for the radar to infill an area of reduced coverage in Scotland within the C-band weather radar network across the British Isles. Comparison to raingauge measurements over this area have shown radar rainfall estimates to be less accurate (Worsfold et al., 2014), particularly on account of the large distance to the nearest C-band radar and also in relation to topography and beam blockage effects (Harrison et al., 2012). The C-band radar network includes four installations in Scotland. Locations of two of them - at Druim a'Starraig (166 km to the northwest of NXPol) and at Hill of Dudwick (95 km to the east) - are marked as blue dots in Fig. 1a. The other two - Munduff Hill and Holehead at distances 161 and 187 km from NXPol respectively - are off the map to the south. Also the locations of raingauges in SEPA's hydrometric network over the study area are shown by green triangles in Fig. 1a.

The study area has several mountainous parts: notably the Cairngorms in the eastern Highlands to the south of NXPol (with the summit reaching 1309 m) and those of the western Highlands to the west (reaching a height of 1150 m within 100 km of the radar site). These lead to radar beam blockages and local orographic enhancements to the precipitation, both of which provide additional challenges for radar QPE (Georgiou et al., 2012). The spatial distribution of annual average rainfall in the region is variable: from less than 700 mm for some areas of the eastern coast, to greater than 3000 mm over some parts of the western Highlands (1981–2010 average precipitation map; Met Office, 2018). An additional challenge is posed by the typically low altitude of the melting layer during winter, which often leads to accumulations of solid precipitation particularly in upland areas. The low melting layer limits the effectiveness of dual-polarisation processing, which is partly based on the electromagnetic scattering properties of liquid precipitation, and is particularly pronounced when the surface topography requires that QPE uses higher altitude radar data. On the other hand, the study area is well suited for assessing precipitation using hydrological models as topography acts as a dominant control on runoff production. The impermeable geology means there are no groundwater transfers between catchments, and the baseflow fraction is low so antecedent condition effects do not persist for extended periods of time. Additionally, the headwater catchments are typically rapidly responding which limits the possible temporal averaging of transient errors in the QPE.

2.2. Description of NXPol QPEs assessed

To deal with mountainous terrain in the vicinity of NXPol, radar scans are taken at different angles relative to the ground. Observations from those scans considered to be at the LUE are combined to create a two-dimensional QPE. Full details of the NXPol radar and its rain-retrieval methods are provided in Neely et al. (2021). Briefly, the system has a 75 kW peak power output split between the two transmit channels, operates using simultaneous transmit and receive (STAR) for dual-polarisation moment estimation, has a 2.4 m antenna leading to a half-power beam width of 0.98° (narrower than most X-band systems), and operates without a radome. In this campaign NXPol collected a volume of observations consisting of ten 360° Plan Position Indicator (PPI) sweeps at increasing elevation angles, including but not limited to 0.5, 1, 1.5, 2, 3, 4°. Each PPI has an azimuthal interval of 1° and a 150 m range-gate spacing to a maximum range of 150 km. The full volume scan cycle took approximately 5.5 min and is labelled in this analysis by the start-time of each volume. Using a static look-up table based on the minimum detectable signal and the occurrence of clutter, each volume of PPIs was collapsed into a single LUE product.

The LUE method described in Neely et al. (2021) differs from the typical radar data gridding approach as it considers the impact of the blocked fraction on the minimum detectable signal with increasing range, rather than using a fixed fraction to eliminate low elevations. It also incorporates the impact of ground clutter on radar data quality, substituting areas that have significantly elevated echo occurrence percentages with data from higher elevation angles. To achieve this, data for each range gate are taken from the lowest elevation that has both a minimum detectable signal of 10 dBZ (factoring in the impact of beam blockage based on a static partial beam blockage correction) and an echo occurrence percentage of less than 75 % based on a static clutter map from six non-consecutive clear-air days. This approach is a necessary compromise between avoiding excessive beam blockage and ground clutter, and the possibility of overshooting of low-lying precipitation for scans with higher angles. The overshooting of precipitation becomes especially problematic behind mountains and is expected to result in a considerable underestimation of the precipitation for catchments with LUE greater than around 3 to 4 km.

A map of catchments used in this study, shaded according to their mean LUE, is shown in Fig. 1b. Regions of high LUE, and anticipated poorer QPE performance, are clearly visible to the south and west. Areas near the radar, and also across the sea to the north, and, to a lesser extent, along the Great Glen (a geological fault line) to the south-west, have lower LUE even for catchments that are a long distance from the radar site.

Ten different NXPol QPEs (summarised in Table 1) were assessed using hydrological simulation in this study. The first five of these methods (R(Z) to R(ZC)) in Table 1) all make use of the Marshall-Palmer
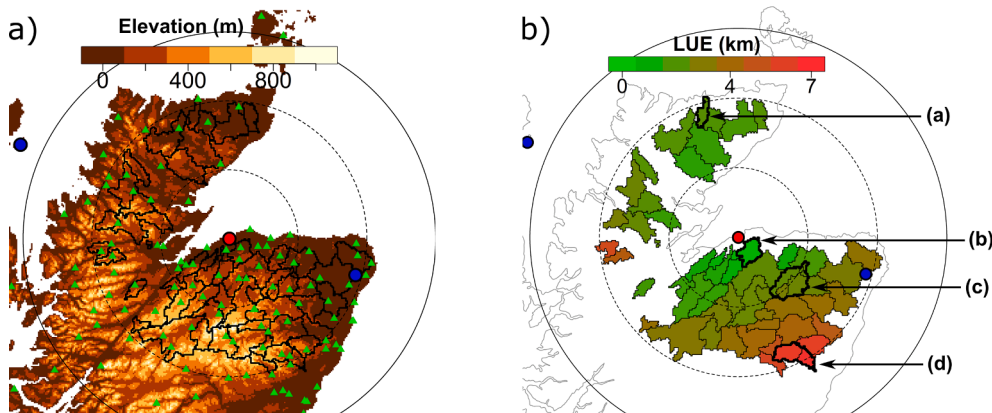

Fig. 1. a) Elevation map of NE Scotland showing the NXPol site (red dot), C-band radar sites (blue dots), and concentric circles indicating distances of 50, 100 and 150 km from NXPol. Black lines indicate the boundaries of the catchments used in this study. Green triangles mark the locations of raingauges. b) The catchments shaded according to their mean Lowest Useable Elevation (LUE) for NXPol. The boundaries of four gauged catchments used as examples are delineated by bold lines, with fine lines showing gauged sub-catchments within them.

Table 1
Description of NXPol QPEs used in this study.

QPE	Description
R(Z)	A simple estimate based on the unfiltered horizontal reflectivity with no post-processing beyond calibration.
R(Z+DTM)	A reflectivity-based estimate with simple clutter mitigation and Digital Terrain Model (DTM) based beam blockage correction.
R(Z+DTM+QC)	As per R(Z+DTM) but additionally removing spurious radar echoes.
R(Z+DTM+QC+At)	As per R(Z+DTM+QC) but applying a dual-polarisation based attenuation correction to the beam blockage correction and reflectivity filter.
R(ZC)	Similar to R(Z+DTM+QC+At) except using a specific attenuation derived clutter map to correct beam blockage.
R(A$_h$)	Specific attenuation is converted into a rain-rate using a fixed R(A) relationship. R(ZC) is used as a fall-back.
R(A$_{h,thr}$)	As per R(A$_h$) except only applying the R(A) relationship where the total differential phase shift exceeds 5°.
R(Z(A$_h$))	Specific attenuation is converted to reflectivity before calculation of the rain-rate. This is used when total differential phase shift is greater than 5°, otherwise R(ZC) is used as a fall-back.
R(KDP-Z)	Smoothly blends an estimate based on the specific differential phase for high-intensity precipitation with the R(ZC) estimate at lower intensities (<20 mm/h).
R(Dual-Pol)	As per R(Z(A$_h$)) except using R(KDP-Z) for infilling.

relationship, $Z = 200R^{1.6}$, between reflectivity, Z, and precipitation rate, R (Harrison et al., 2012; Marshall and Palmer, 1948) but represent a progression of increasing data processing. This starts with R(Z), which simply applies the Marshall-Palmer relationship to the calibrated horizontal reflectivity as measured by NXPol, thus providing a baseline for the assessment of all other methods. The second method, R(Z+DTM), applies a partial beam blockage correction based on a Digital Terrain Model (DTM) to the horizontal reflectivity before precipitation estimation. This method is implemented using wradlib (Heistermann et al., 2013) using 1 arc-second SRTM (Shuttle Radar Topography Mission) data for the surface topography. R(Z+DTM+QC) additionally applies dual-polarisation quality control (QC), removing second trip echoes and non-meteorological echoes using a fuzzy logic approach followed by removal of isolated pixels using connected component labelling (Dufton and Collier, 2015; Dufton, 2016). R(Z+DTM+QC+At) then applies attenuation correction through the implementation of the ZPHI method (Testud et al., 2000). In this instance a minimum precipitable path length of 3 km (10 continuous range gates identified as meteorological by the fuzzy logic QC) is required for data assumed to be below the melting layer based on extrapolation of surface temperature data using a fixed lapse rate of 6 °C/km. Differential phase shift is smoothed using a modification of the Hubbert and Bringi (1995) iterative method prior to identification of the phase limits for the calculations (Dufton, 2016). The method assumes a constant factor of 0.27 dB/deg to estimate specific attenuation from specific differential phase (also used in later methods for direct precipitation estimation). R(ZC) is identical to the previous method with the exception of the partial beam blockage correction being applied. In this case the correction is derived from the consistency of polarimetric variables during the summer of the RAiNS deployment, as proposed by Diederich et al (2015a). This leads to higher estimates of the correction needed when compared to the DTM approach: see Neely et al. (2021) for more details.

The next five methods make use of either specific attenuation, specific differential phase or both to calculate the QPEs, with R(ZC) being used as an infill when these methods are not possible (above the melting layer in the case of specific attenuation, for example). R(A$_h$) estimates precipitation intensity using specific attenuation, A_h, assuming an atmospheric temperature of 10 °C leading to a relationship of $R = 45.5A_h^{0.83}$ (Diederich et al., 2015b) where A_h is estimated during attenuation correction by the ZPHI method. R(A$_{h,thr}$) is identical to R(A$_h$) when the total differential phase shift along the rain region path identified exceeds 5°, but otherwise defaults to R(ZC). Considering this method allows an assessment of the impact of potentially spurious results during light rainfall conditions where noise in the differential phase shift measurements could have a significant impact. R(Z(A$_h$)) uses the same 5° threshold on the total differential phase shift used with R(A$_{h,thr}$) but instead converts A_h into a synthetic equivalent horizontal reflectivity, $Z_{h,syn}$, for use in the Marshall-Palmer relation. This is the same approach taken to derive the dual-polarisation beam blockage correction introduced in the R(ZC) method. This approach acts as a dynamic bias correction to reflectivity, while still using the Marshall-Palmer

relation, which is a good climatological fit for UK precipitation estimation. R(KDP-Z) instead focuses on using specific differential phase, K_{dp}, for the estimation of precipitation. Here the method uses the relationship from Ryzhkov et al. (2014) where the estimates are blended with those from R(ZC) at all K_{dp} estimated precipitation intensities between 10 and 20 mm h^{-1} using a linear weighted average. Below 10 mm h^{-1}, R(ZC) is used without K_{dp} input. The weighting accounts for the well-known difficulties of estimating small values of K_{dp} (Vulpiani et al., 2012). The final method, R(Dual-Pol), is a combination of R(Z(A$_h$)) and R(KDP-Z) where specific attenuation based estimates are used as first preference, followed by those utilising specific differential phase, and finally reverting to reflectivity where these estimates are not available. All QPE methods are applied to the published calibrated NXPOL radar dataset, where horizontal reflectivity is calibrated using polarimetric self-consistency and differential reflectivity is calibrated using vertically pointing radar scans (Bennett, 2019; Neely et al., 2021). Since specific attenuation and specific differential phase are immune to radar miss-calibration, QPE methods involving them will be less sensitive to any temporal variations in radar calibration over the study period. All NXPol radar data processing is coded in python, taking advantage of the open source libraries Py-Art (Helmus and Collis, 2016) for reading and writing CfRadial files and wradlib (Heistermann et al., 2013) for DTM estimation and gridding of the data. No raingauge or climatological adjustments are applied to the NXPol-derived QPEs to avoid confounding the current analysis which is focussed on comparing QPEs of increasing complexity in their use of radar variables. The strategic aim is to develop an X-band radar processing chain to which additional corrections can be applied and assessed as part of a staged, evolutionary process. This allows for consideration of raingauge data at a later stage, perhaps as part of a wider multi-sensor network.

QPE products were produced for two periods in 2016: Period 1 from 1 March to 30 April and Period 2 from 1 June to 17 August, with an interval of down-time for the radar in between. The melting layer was typically much lower during Period 1, with median heights of 1043 and 2243 m for the two periods respectively: this results in much more frequent use of R(ZC) as a fall-back for the dual-polarisation QPEs over Period 1.

For use with the G2G distributed hydrological model, the LUE products created on the native polar coordinate system of the NXPol were regridded onto a 1 km Cartesian rectilinear grid using the area-weighted average of all 2D polar radar pixels intersecting with each Cartesian grid-cell. Missing and filtered radar pixels within a grid-cell are excluded from the average provided they cover less than 30 % of the area, after which they are set to NaN and counted as having zero precipitation by G2G. The resulting rectilinear coordinate system is the same as used by the network C-band QPE product. To produce continuous QPEs for use in the hydrological model, any period of greater than 10 min without NXPol data was infilled using QPEs from the C-band network. This included the entire month of May (between Period 1 and 2), which was subsequently excluded from the analysis of river flow. Apart from during May, C-band QPE data were only used 314 times for

infilling, of which 275 were used during a 23-hour period of downtime between 6 and 7 April. C-band data, as opposed to raingauge data, were chosen for infilling so as not to bias comparisons between NXPol and C-band QPEs. The irregularly timed QPEs (approximately 5.5 min apart) were accumulated using a simple trapezoidal rule, without allowing for advection effects, to produce 15-minute precipitation totals for input to G2G. Experience in a UK context has shown that accounting for the movement and development of storms between time-steps (see, for example, Fabry et al. (1994)) normally has little impact on modelled river flows for the catchment scales considered here (median catchment area 232 km^2).

3. Alternative precipitation sources for comparison

3.1. R(C-band) precipitation

The UK Met Office operates four C-band radars in Scotland as part of a wider network of 18 weather radars across the British Isles. Data from the radars are processed by the Radarnet IV Central Processing System at Exeter (Met Office, 2020) to produce an estimate of rainfall intensity at ground level. The processing includes clutter removal, beam blockage correction, correcting for attenuation and the vertical profile of reflectivity (VPR), adjusting for orographic enhancement, and correcting for residual bias using observations from the raingauge network (Harrison et al., 2006; Darlington et al., 2016a,b). These corrected data are then composited into a UK-wide gridded precipitation product.

The gridded C-band rainfall intensity data used in this study were sourced from a live data-feed supplied by the Met Office on a 1 km Cartesian grid with a 5 min time-step. These data are identical, up to minor differences in the occurrence of missing data, to the 1 km resolution UK Composite Rainfall product available from the CEDA Archive (Met Office, 2003). These gridded time-series were accumulated (without accounting for advection, as per NXPol QPE) to form a C-band QPE of 15-minute rainfall totals on a 1 km grid for input to the G2G hydrological model.

While there are several processing elements in common between NXPol and the operational C-band processing, the latter includes a greater use of external data sources including weather model fields for VPR correction and orographic enhancement adjustment, and raingauges for bias correction (Harrison et al., 2009, 2012; Georgiou et al., 2012).

3.2. Raingauge precipitation

Raingauge data from SEPA's hydrometric network were used to produce gridded 15-minute rainfall accumulation estimates for the whole of Scotland, including the study area, on a 1 km grid. This used a multiquadric interpolation technique (Hardy, 1971) in an extended form (Cole and Moore, 2008) employing a Euclidean measure of distance and zero "offset" which is equivalent to Kriging with a linear variogram (Borga and Vizzaccaro, 1997). Quality control of the raingauge data was performed as an initial step using the methods presented in Howard et al. (2012). This precipitation estimate provides a useful baseline, one previously found to produce the best modelled river flow and subsequently chosen for calibration of the G2G model (Cole and Moore, 2009).

For the study period, the raingauge network consisted of approximately 290 tipping-bucket raingauges over the whole of Scotland, and over the studied catchments a mean gauge density of approximately-one raingauge per 290 km^2 (calculated using the ArcMap point density tool with a 20 km neighbourhood). Raingauge locations within the study area are mapped in Fig. 1a.

4. The G2G model

The Grid-to-Grid (G2G) model is a distributed physical–conceptual

hydrological model (Bell et al., 2009; Environment Agency, 2007, 2010; Moore et al., 2006) used for a range of research and operational applications including flood forecasting by both the Scottish Flood Forecasting Service (Cranston et al., 2012) and the Flood Forecasting Centre for England and Wales (Price et al., 2012). G2G is underpinned by spatial datasets on landscape properties (elevation, soil/geology and land-cover) in support of its area-wide application, and also employs precipitation, potential evaporation and air temperature as gridded time-series inputs. To account for sub-grid heterogeneity, the Probability Distributed Model (PDM; Moore 1985, 2007) concept is employed within each grid-cell to generate surface and subsurface runoff components. These runoffs are routed along separate water pathways from grid-cell to grid-cell to produce hillslope, river channel, and groundwater flows; return flows from the groundwater and soil water to the surface water pathway are also represented. The G2G model is based on water conservation principles with its water balance updated at each time-step.

The G2G setup used in this study follows the version used operationally by the Scottish Flood Forecasting Service. It runs with a model time-step of 15 min and includes use of the G2G Snow Hydrology module based on the PACK snowmelt model (Moore et al., 1999). Although the use of spatial datasets of landscape properties reduces the importance of calibration compared to lumped conceptual hydrological models, simulation-mode calibration was used to improve G2G operational performance. A number of parameters relating to runoff production and routing were calibrated across the whole model domain of Scotland (rather than just the study area), using river flow observations from January to September 2016. Additionally, a further two parameters (controlling channel roughness and return flow from soil water) were adjusted separately for each gauged catchment. Calibration paid attention to performance over the full flow range as well at high flows, relevant to its use for flood forecasting, and employed a mix of visual and automated calibration tools. Gridded raingauge precipitation was used as input (Section 3.2). Whilst data assimilation of river flow observations is used to enhance model performance for operational flow forecasting purposes, it is not invoked here so as not to confound the comparative assessment of simulated river flow using the different QPEs as input to G2G. The PACK formulation (Moore et al., 1999) of the G2G Snow Hydrology module acts as pre-processing step affecting the input precipitation. Air temperature is used as a threshold to differentiate between liquid and solid precipitation and also to control the melting process through a temperature-excess formulation; the storage and release of water in the snowpack is also represented.

The potential evaporation (PE) and air temperature inputs used here are those employed in G2G operationally. For PE, a standard annual profile grid of monthly averages was employed, calculated as the monthly average MORECS PE (Thompson et al. 1981; Hough and Jones, 1997) using the 40 km gridded monthly values over the 1981 to 2010 period. Air temperature was from the Post Processing of the UK Met Office weather prediction model (UKPP) for a height of 1.5 m and obtained at a 2 km and hourly space–time resolution. Data were downscaled to a 1 km grid using a lapse rate of 5.9 °C/km to account for differences in mean elevations between the 2 and 1 km grid-cells.

5. Catchment selection and river flow data

Fig. 1 maps the 57 gauged catchments and sub-catchments selected for inclusion in this study. These were chosen from an original selection of 63 catchments having a mean distance of less than 100 km to the radar site and of interest to SEPA. Of the original 63 catchments, two were discounted due to missing river flow observations and two more through inspection of hydrographs revealing significant sub-daily fluctuations that were attributed to measurement error. A further two sites were discounted as G2G simulated flows were found to perform poorly regardless of precipitation input type. The river flow data at 15 min intervals were obtained from SEPA.

6. Performance statistics used for hydrological assessment of QPEs

To describe the performance of the modelled river flows and, by extension, that of the precipitation estimates used to produce them, several statistics are employed. Each compare modelled flows to observations, and each aim to capture a different aspect of performance.

One statistic, the R^2 Efficiency - also known as the Nash-Sutcliffe Efficiency (Nash and Sutcliffe, 1970) - is defined as

$$R^2 = 1 - \frac{\sum (Q_t - q_t)^2}{\sum (Q_t - \overline{Q})^2}. \tag{1}$$

Here q_t and Q_t are, respectively, the modelled and observed flow at time-step t, and $\overline{Q}$ is the mean observed flow over the period. This commonly used statistic places a higher weight on the larger absolute discrepancies that are typically found for high flows. As such, it is particularly useful in assessing the high flow regime and as an indicator of an input precipitation's suitability for use in flood modelling. An R^2 Efficiency of 1 indicates a perfect agreement between modelled and observed flows, whilst a value of less than zero indicates that the performance, as measured by mean square error, is worse than would be obtained by using the observed mean flow value. Note that R^2 Efficiency differs in its definition from the coefficient of determination r^2, where r is the correlation coefficient, which does not account for bias effects on model efficiency and therefore has a larger or equal value.

The correlation coefficient, r, is also calculated. This statistic is insensitive to overall absolute and relative (linear) biases in the modelled river flow. As such, it may also be less sensitive to bias corrections and other compensations applied to the QPEs, such as those featuring in the network C-band but not the NXPol. Correlations have values between $+1$ for a perfect positive correlation and -1 for a perfect negative correlation, with zero indicating no correlation.

The modified Kling–Gupta Efficiency (Gupta et al., 2009; Kling et al., 2012) is defined as

$$KGE' = 1 - \sqrt{(r-1)^2 + (CV_q/CV_Q - 1)^2 + ((\overline{q}/\overline{Q}) - 1)^2} \tag{2}$$

with CV_q and CV_Q the coefficient of variation (standard deviation divided by mean) for the modelled and observed flows respectively, and $\overline{q}$ the mean modelled flow over the evaluation period. This statistic obtains its maximum value of 1 for perfect agreement between model and observation. In this study KGE' is applied to the square-root of river flow, denoted as KGE'[sqrt], in order to produce a general metric that places weight on low and medium flows as well as high flows: it therefore may be sensitive to features in the river flow not adequately captured in the R^2 Efficiency.

The percentage bias, $100(\overline{q}-\overline{Q})/\overline{Q}$, in the modelled flow compared to the observation is also calculated. This statistic should approximate the relative bias in the input precipitation because of: (i) the conservation of water within the G2G model, (ii) the relatively low contribution of evaporation to the water balance for the humid temperate climate of Northern Scotland, (iii) the small groundwater component of river flow, and (iv) the relatively long time-span of the study period compared to typical hydrological response times of the catchments.

Unless stated otherwise, all performance statistics are evaluated at the model time-step of 15 min over the period 1 February to 17 August 2016, excluding the month of May (for which all NXPol QPEs were missing and infilled using R(C-band): see Section 2). The G2G simulations were started on 1 February 2016 with each selected precipitation input. To avoid the uncertainty associated with a cold start, and possibly poorly initialised water stores in the model, model states that had been spun-up using raingauge precipitation from a start on 10 October 2013 were used.

Statistics are also used to quantify the influence of snow accumulation and melt on river flow. This involves calculating the fraction of days for which modelled flows with gridded raingauge data as input differ by more than 20 % when the G2G Snow Hydrology module is included (as is standard) or excluded (all precipitation is treated as rainfall). This statistic naturally captures the full impact of snow on flows including its accumulation, melt, rain-on-snow events, the influence of different elevations within a catchment, and how this translates into river flows.

7. Performance assessment

The performance of the NXPol R(Dual-Pol) QPE, which makes full use of dual-polarisation variables, is assessed first. Each catchment in Fig. 2 is shaded according to the R^2 Efficiency, correlation, and bias of G2G modelled flows using the NXPol R(Dual-Pol) QPE as input. Except for a few catchments very close to the radar, and with reference to the LUE map in Fig. 1b, the catchments with highest R^2 Efficiency and highest correlation coefficient are typically those with lower LUEs. In contrast, those catchments with high LUEs (exceeding 4 km) have, without exception, a strong negative bias (worse than −50 %) and a correspondingly poor R^2 Efficiency (below zero), indicating that a large portion of the precipitation for these catchments is missed by the R(Dual-Pol) QPE. The correlation for these catchments is also often poor (usually less than 0.5).

Modelled river flows, calculated using either R(Dual-Pol) QPE or raingauge QPE - for the four example catchments delineated by bold lines in Fig. 2 and labelled on Fig. 1b - are compared to observed flows in the hydrographs of Fig. 3. Time-series of catchment average precipitation and air temperature are also displayed in the figure while catchment details and analysis statistics are summarised in Table 2. These catchments were chosen to represent the range of behaviours found in modelled river flows using NXPol-derived QPEs as input. In all four cases, the use of raingauge precipitation produces modelled river flows that compare at least reasonably well to the observations ($R^2 > 0.6$, $r > 0.8$, |bias|<20 %, in all cases, see Table 2). For NXPol QPEs, the range of behaviour may be summarised as follows.

Strathy at Strathy Bridge (Fig. 3a). A catchment in the far north of Scotland which is distant (92 km on average) from NXPol but has a fairly low mean LUE (2.1 km). The R^2 Efficiency (0.43) and correlation coefficient (0.68) of modelled flows using R(Dual-Pol) QPE are reasonable for this catchment suggesting that LUE has a greater influence on performance than range from the radar, at least up to distances of around 100 km. The total catchment average precipitation recorded in R(Dual-Pol) (321 mm) is 14 % lower than that found using raingauge precipitation (373 mm) which feeds through to a bias of −14 % in modelled flows using R(Dual-Pol) (Table 2). Also note that throughout Period 1 the catchment's mean air temperature at ground level is often no more than a few degrees above 0 °C. This has two consequences. Firstly, the catchment's mean air temperature is frequently below the threshold of 0.75 °C at which G2G treats precipitation inputs as snow – and it will tend to be significantly colder than this at the catchment's higher elevations. This translates into a reasonable impact of snow on the river flows (determined as the percentage of days for which the modelled flows with and without the inclusion of snow processes differ by more than 20 %, see Table 2), even for this relatively low elevation catchment. The other example catchments are also affected by snowfall to a degree partially determined by their elevation (see Table 2). Secondly, above the catchment, the low height of the melting layer almost totally prevents the calculation of the specific attenuation, which is based on the properties of liquid water. Hence, R(Dual-Pol) will be identical to R(KDP-Z) for almost all of Period 1 for this catchment. Any period for which the height of the melting layer prevents the calculation of specific attenuation over more than 50 % of a catchment is shaded red on the hyetograph for R(Dual-Pol) in Fig. 3. Note that additional checks in the processing chain for radar signals associated with solid precipitation may also limit the calculation of specific attenuation, so this measure provides only a maximum possible percentage. The other example catchments are also affected by this to a degree mainly
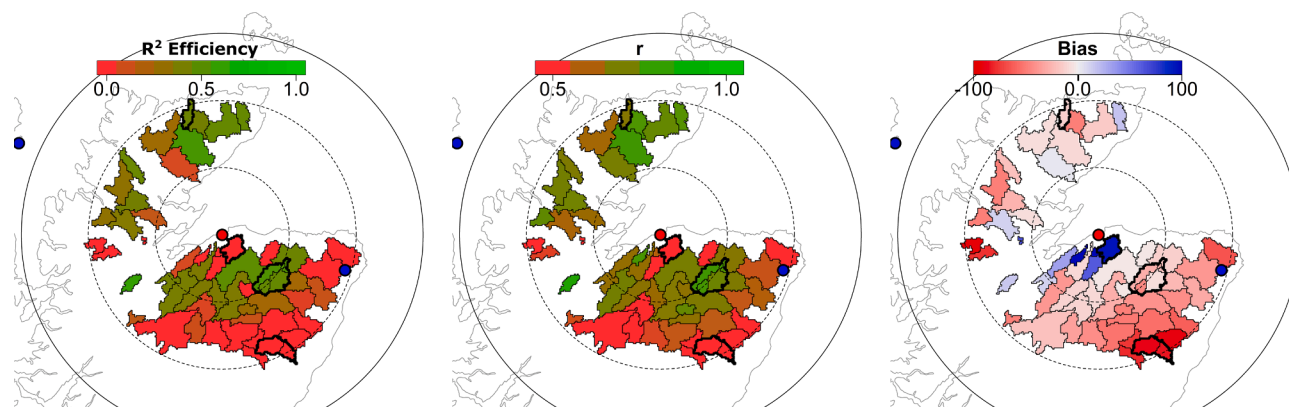
Fig. 2. Performance of G2G modelled river flows using the R(Dual-Pol) QPE. Each catchment is coloured according to the performance metric used: R^2 Efficiency, correlation coefficient (*r*), or percentage bias. An R^2 Efficiency of less than zero is set to zero for clarity.

determined by their mean LUE.

Lossie at Sheriffmills (Fig. 3b). A catchment very close to the radar (14 km) and having a low LUE (0.5 km). Modelled river flow using the R(Dual-Pol) QPE displays a very large overall positive bias (+94 %), which is far more pronounced in Period 1 (+164 % bias) than Period 2 (+30 % bias), and arises from catchment-average R(Dual-Pol) precipitation totals that are a very large compared to raingauge precipitation totals (40 % larger for the full period or 120 % larger for Period 1). Nevertheless, even in Period 1, modelled flows using R(Dual-Pol) data agree reasonably well with the observed flows in terms of relative magnitude and timing of the flood peaks. Similar behaviour (biases in excess of 90 %) is found for all three catchments closest to NXPol. This was traced to a previously undiagnosed antenna elevation pointing error in Period 1, leading to overcorrection of beam blockage for this period, especially when using beam blockage corrections derived using data from Period 2 (Neely et al., 2021). This effect was strongest close to the radar where the LUE derivation incorporated a greater number of radar voxels from lower elevations which suffered more from the overcorrection.

Deveron at Avochie (Fig. 3c). A catchment fairly close (51 km) to the radar and with a relatively low mean LUE (2.3 km), producing reasonable modelled river flows. The highest peak in the observed flow data, reaching 127 m^3/s at 19:30 15 June, is the most significant flood peak found during the study period at an example catchment: it is the only peak that approaches the median annual flood (129 m^3/s for this catchment, see Table 2). This peak is underestimated in both the modelled flow using the raingauge QPE as input (peak of 53 m^3/s) and the R(Dual-Pol) QPE as input (peak 41 m^3/s). The difference appears to reflect the different catchment-average total precipitation recorded over the preceding 48 h (51 mm for raingauge and 38 mm for R(Dual-Pol)). Over the whole study period however, the total precipitation recorded for this catchment is quite similar for the two QPEs: 424 mm for raingauge and 409 mm for R(Dual-Pol).

North Esk (Tayside) at Inveriscandye (Fig. 3d). A catchment in the south of the radar area that is both a long distance (94 km) from NXPol and on the far side of the Cairngorm mountain range. Its mean LUE of 6.7 km is the highest of all the catchments included in this study. Because of this, the radar beam overshoots almost all precipitation in this catchment (total catchment-average R(Dual-Pol) precipitation is just 55 mm) resulting in a large negative bias in the modelled flow (-84 %). Similar behaviour is seen for all catchments with LUE exceeding 4 km.

7.1. Influence of LUE and range of the radar observations on performance

Fig. 4a-c show scatter plots of R^2 Efficiency, correlation coefficient, and bias for modelled river flow using either R(Dual-Pol) or raingauge

QPE as input against each catchment's mean LUE. The plots for correlation coefficient and bias (Fig. 4b,c) also show the linear least-squares regression line and associated coefficient of determination, denoted by ρ in this context. For R(Dual-Pol) QPE, the systematic reductions in correlation coefficient and bias is particularly striking and is reflected by strong coefficients of determination for the least squares regression lines: 0.38 and 0.63 for the correlation coefficient and bias, respectively. Similarly strong fits (in the ranges 0.38 to 0.61 and 0.51 to 0.63 for the correlation coefficient and bias, respectively) are found for all NXPol QPEs. The lack of similar behaviour in modelled river flow using raingauge QPE (hollow grey circles in Fig. 4b,c) shows that the trends with R(Dual-Pol) are not associated with the characteristics of the hydrological catchments themselves. The trend for R^2 Efficiency is more complicated, which instead tends to have largest values at LUEs of around 2 km for which biases of around zero are typical.

The existence of distant catchments that perform comparatively well with NXPol precipitation, such as the Lossie at Sheriffmills (Fig. 3b), suggests that it is LUE rather than range that is chiefly responsible for the deterioration of performance shown in Fig. 4a-c. Nevertheless, the LUE is correlated with range having a value of $r = 0.68$. Catchments at closer range will benefit from lower minimum detectable signal, a smaller areal resolution, and suffer less from partial beam filling. Weaker values of the coefficient of determination for the regression lines (0.084 for r and 0.56 for bias using R(Dual-Pol)) obtained when mean range is used as the explanatory variable, rather than mean LUE, suggest it is LUE that has the strongest influence.

7.2. Comparing different QPEs for Period 1 and Period 2

The boxplots of Fig. 5a summarise the overall performance of all QPEs, as assessed by statistics calculated on the modelled river flows and using data from both Period 1 and Period 2. Statistics are only shown for those 38 catchments with an LUE of less than 3 km in altitude on average across the catchment. Similar trends are repeated if all 57 catchments are included (not shown) - albeit with an overall reduction in R^2 Efficiency, correlation, and bias for all NXPol QPEs - due to the inclusion of poorly performing catchments whose high mean LUE would flag them as unsuitable.

The raingauge QPE tends to produce the best modelled river flows according to the R^2 Efficiency metric. Some of this improvement could be due to the G2G hydrological model having been calibrated using raingauge QPE as input. But this seems unlikely to account for a large proportion of the difference, especially given the reduced role of calibration for an area-wide distributed model like G2G compared to, for example, a lumped hydrological model with a catchment-specific calibration. The R^2 Efficiency also indicates a general improvement in performance with either increased processing complexity for single
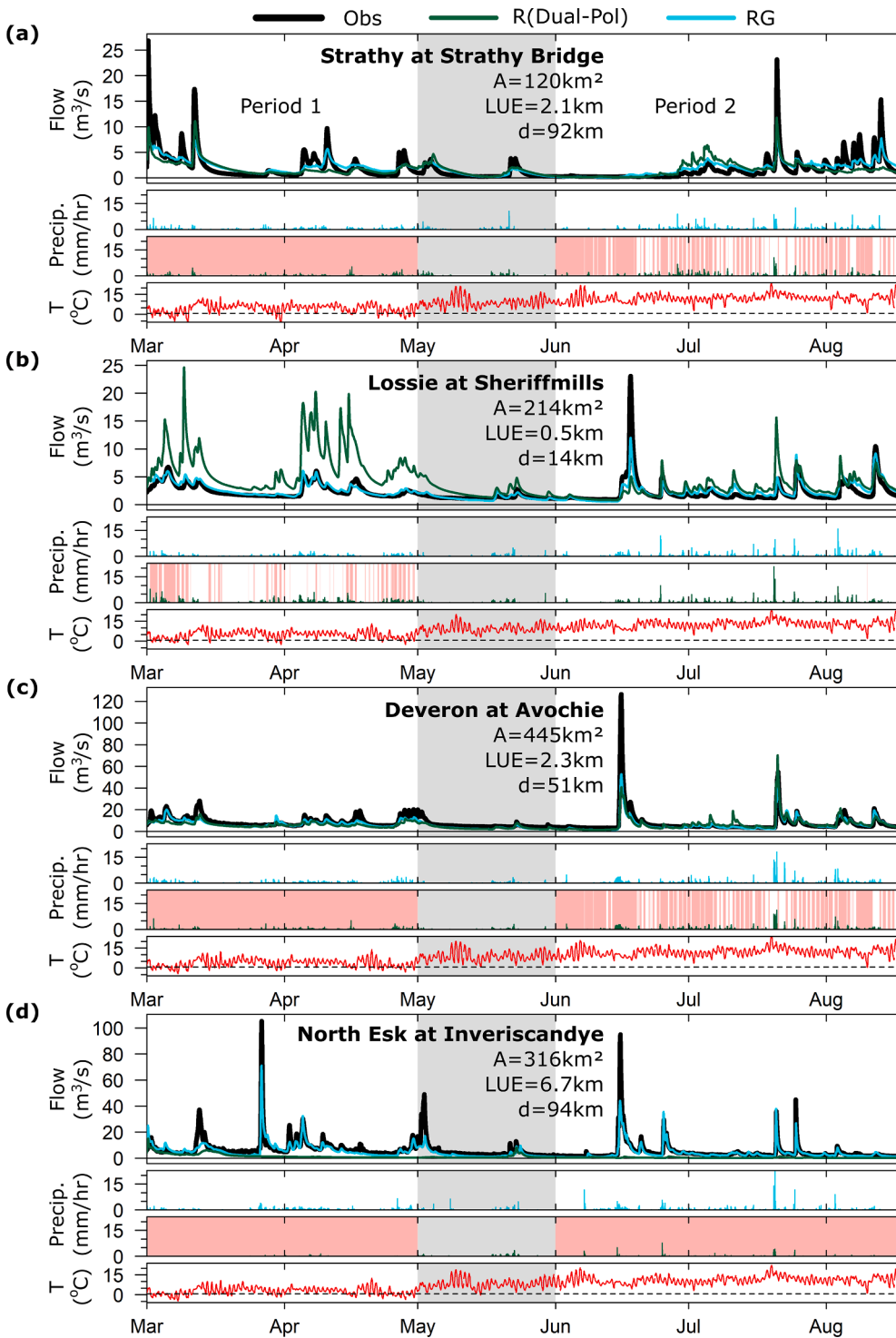
Fig. 3. Time-series displays for the example catchments, each containing graphs of river flow along with catchment-average precipitation - from raingauges and R(Dual-Pol) radar - and air temperature. **Graph 1.** Observed (black) and modelled (green: R(Dual-Pol), cyan: raingauge) river flow. The G2G catchment area, mean LUE and mean distance from NXPol is given below the catchment (river and station) name. Grey shading indicates a period of downtime for NXPol, infilled using R(C-band) precipitation). **Graph 2.** Raingauge precipitation. **Graph 3.** R(Dual-Pol) precipitation. Red markers indicate when the bottom of the melting layer is lower than the LUE over greater than 50 % of the catchment. **Graph 4.** Air temperature at screen height (1.5 m). Precipitation at temperatures below 0.75 °C (highlighted as a dashed horizontal line) is treated as snowfall in G2G.

polarisation QPEs (R(Z) to R(ZC) in Table 1), or using the dual-polarisation estimates (R(A$_h$) to R(Dual-Pol) in Table 1), albeit with the R(ZC) QPE able to match the performance of some dual-polarisation estimates. Correlation, KGE'[sqrt] and bias generally repeat the same trends towards improvement found for R^2 Efficiency, but with some exceptions. The strongest increase in performance is seen for the bias. This suggests that the improved bias is the factor responsible for a larger part of the improvement seen in R^2 Efficiency (which can be viewed as a combination of correlation, bias, and the ratio of standard deviations (Gupta et al., 2009)). It also suggests that while the application of a bias correction to NXPol QPEs should be expected to increase the overall

R^2 Efficiency for their associated modelled river flows, it may reduce the further improvements gained by processing complexity or dual-polarisation.

The boxplots of Fig. 5b,c highlight the different trends in performance found using the radar QPEs for Period 1 (March to April) and Period 2 (June to August). There is also a difference across the two periods in the performance of modelled river flow using raingauge or R(C-band) QPE as input to G2G. Part of the difference for both radar and raingauge inputs may be due to the increased complexity of modelling snow accumulation and melt within the G2G model. One way to quantify this is by comparing G2G modelled flows (with raingauge QPE as

Table 2

Catchment details and analysis statistics for the four example catchments.

	Strathy at Strathy Bridge	Lossie at Sheriffmills	Deveron at Avochie	North Esk at Inveriscandye
Catchment Details				
National River Flow Archive ID*	96003	7003	9001	–
Catchment Area (from G2G), km^2	120	214	445	316
Mean NXPol LUE, km	2.1	0.5	2.3	6.7
Mean distance from NXPol, km	92	14	51	94
Mean (min, max) elevation, m†	165 (36, 312)	185 (25, 423)	329 (107, 680)	458 (46, 836)
Median annual flood, m^3/s*	50	44	129	–
Max observed flow in study period, m^3/s	27	23	127	105
Split Period Analysis				
A_h potential availability, % Period 1 (Period 2)	0 (39)	70 (100)	1 (35)	0 (0)
% of flow affected by snow Period 1 (Period 2)	7 (0)	1 (0)	19 (0)	49 (0)
Full Period Analysis (excluding May)				
Total precipitation, mm Dual-Pol (RG)	321 (373)	527 (377)	409 (424)	55 (387)
R^2 Efficiency R(Dual-Pol) input (RG input)	0.43 (0.60)	−3.52 (0.72)	0.52 (0.68)	−0.41 (0.76)
r R(Dual-Pol) input (RG input)	0.68 (0.84)	0.42 (0.86)	0.76 (0.88)	0.17 (0.90)
% bias R(Dual-Pol) input (RG input)	−14 (1)	94 (8)	−21 (−18)	−84 (−15)

*Source: National River Flow Archive (NRFA), https://nrfa.ceh.ac.uk.
†Calculated from 1 km average elevation grid used in G2G Snow Hydrology module.

input) calculated either using the G2G Snow Hydrology module (as is standard), or excluding it (when all precipitation is treated as rainfall). On average across all catchments, river flows calculated using these two model setups differ by more than 20 % for 31 % of days in Period 1, compared to almost no differences of this size (0.1 % of days) for Period 2. Additionally, the short time periods over which river flows have been modelled can make results sensitive to the observed weather conditions.

For the NXPol QPEs, the clearest difference between the two periods is the lack of improvement produced by the increasing use of dual-polarisation in Period 1, compared to the strong improvements found for Period 2. This is attributed to the considerably lower height of the melting layer in Period 1, which limits the occurrence of the liquid precipitation conditions assumed in the use of estimators based on specific attenuation, variations of which are the main difference between the dual-polarisation methodologies. Fig. 6 shows the distribution of the highest altitude for which the specific attenuation is calculated, which is 250 m below an estimated 0 °C height. In Period 1 this averages a median of just 793 m, compared to 1993 m in Period 2, and leads to at least 35 % of the radar domain never having estimates based on specific attenuation available in the first period (compared to less than 10 % in the second period). The trend for improvement produced by increasing processing complexity and use of dual-polarisation for Period 2 is consistent with that found by Neely et al. (2021; Fig. 5 therein) where

the same QPEs were assessed against raingauge data. However, use of hydrological model simulations of river flow against observations for assessment of the different QPEs, when employed as alternative model inputs, produces a much stronger contrast in performance between methods particularly when considering the correlation and bias. This results from the greater spatial coverage of the hydrological catchments when compared to raingauges, which can be subject to localised error structures. This furnishes further evidence of the benefit of using catchment-scale river flow data alongside direct raingauge data comparisons for assessing radar QPE. The increased correlation of the R(A_h) and R($A_{h,thr}$) methods for multiple catchments when compared to R(ZC) in Period 2 is further evidence that estimators based on specific attenuation are impacted to a lesser extent by variability in the drop-size distribution of the precipitation than conventional ones employing reflectivity (Diederich et al., 2015b; Chen et al., 2021).

7.3. Mapping best performing QPEs

Fig. 7 maps the best performing NXPol QPE - as determined by either R^2 Efficiency, correlation or bias on modelled river flow - for the full study period. The lowest absolute values of bias are almost exclusively found for R(KDP-Z) or R(Dual-Pol). For a number of catchments, these two QPEs give identical performances. In general, even when not exactly equal, their performance is very similar: 90 % of catchments have an
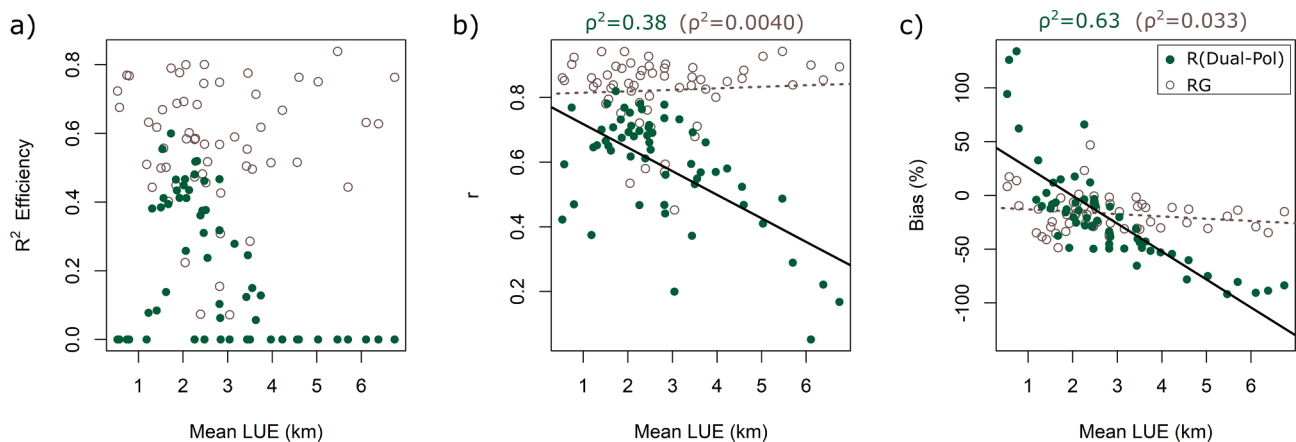

Fig. 4. Scatter plots showing (a) R^2 Efficiency, (b) correlation coefficient, r, and (c) percentage bias in modelled river flow using R(Dual-Pol) (green circles) or raingauge (hollow grey circles) QPEs as input. Values of R^2 Efficiency less than zero are set to zero for clarity. Straight lines in (b) and (c) indicate the linear least-squares regression line - for either R(Dual-Pol) (solid black line) or raingauge (dashed grey line) QPEs as input - with the associated coefficient of determination, ρ^2, shown above the plot (that for raingauge QPE input is in brackets).
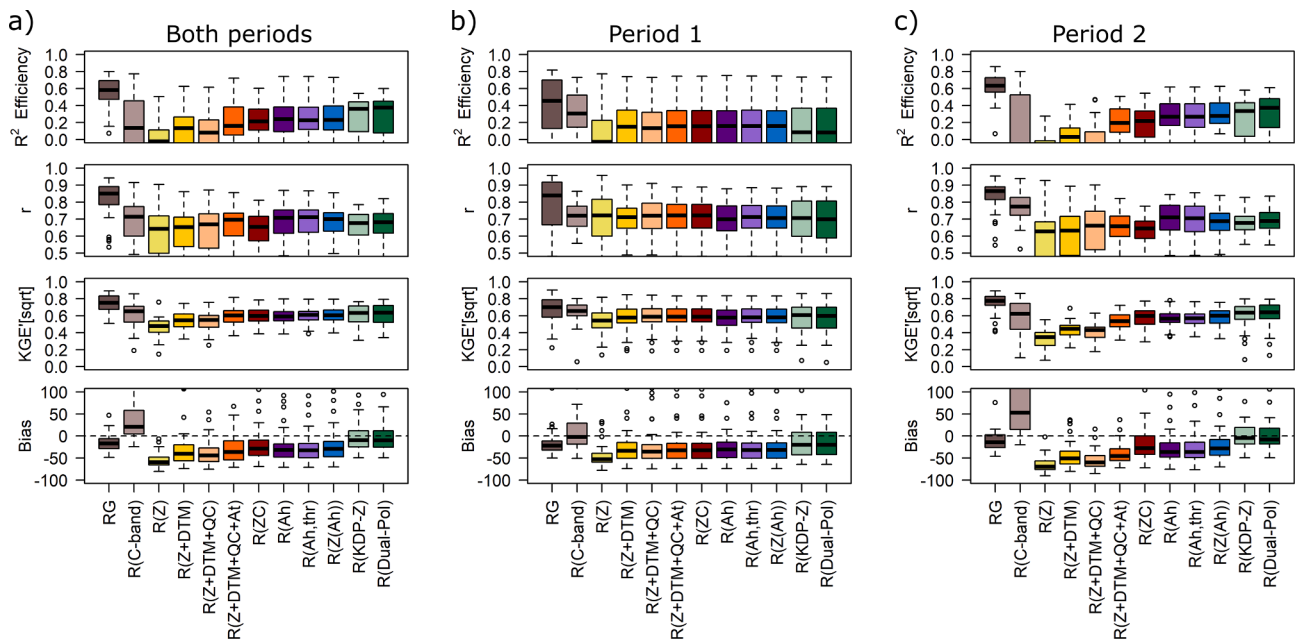
Fig. 5. Boxplots summarising the performance of modelled river flow for the 38 catchments with a mean LUE less than 3 km, separately for the whole study period (left), Period 1 (March to April, centre) and Period 2 (June to August, right) for all precipitation inputs. The coloured box displays the interquartile range, the median is shown as the horizontal black line therein, and the typical range of the statistic is shown as black dashed lines extending to a maximum of 1.5 times the interquartile range with outliers beyond this range shown as hollow circles.

absolute difference in percentage bias between these QPEs which is smaller than 2 %. Their performances assessed by correlation or R^2 Efficiency are also very similar.

The typically lower absolute bias in R(KDP-Z) and R(Dual-Pol) feeds through into typically superior R^2 Efficiency. However, when judged by correlation coefficient the picture is far more mixed: various dual-polarisation or non-dual-polarisation QPEs are found to give the best performance, especially for some of the catchments with lower LUE. When judged by median correlation coefficient for catchments with LUE below 3 km (Fig. 5a), R(Z+DTM+QC+At), R(A$_h$), R(A$_{h,thr}$), and R(Z (A$_h$)) QPEs all perform better than R(KDP-Z) and R(Dual-Pol). These results broadly reflect those shown in Fig. 7 of Neely et al. (2021) where the various NXPol QPEs were assessed against raingauge measurements.

Fig. 8 maps in green the catchments for which the performance of R(Dual-Pol) is better than R(C-band). The R(Dual-Pol) QPE has a higher R^2 Efficiency than R(C-band) for 23 catchments that tend to be either near the radar, or towards the south-east and north. This is expected as LUE for the NXPol radar is low for these locations while, due the distance to the nearest C-band radar and the intervening topography, observations contributing to the C-band QPEs will be from higher altitudes. The three catchments close to the radar and suffering high positive bias in R(Dual-Pol) as a result of the antenna elevation pointing error in Period 1 are an exception. A similar pattern of best-performing catchments is also seen for the bias. This overall behaviour is the result of averaging the differing behaviours in Periods 1 and 2, as shown in Fig. 5. In Period 1 the benefit of using the dual-polarisation variables in the NXPol QPE are limited, and the R^2 Efficiency of R(Dual-Pol) is only better than that of R(C-band) for 10 catchments. In contrast, during Period 2, R(Dual-Pol) has better R^2 Efficiency than that of R(C-band) for 30 catchments as the increased use of dual-polarisation variables for
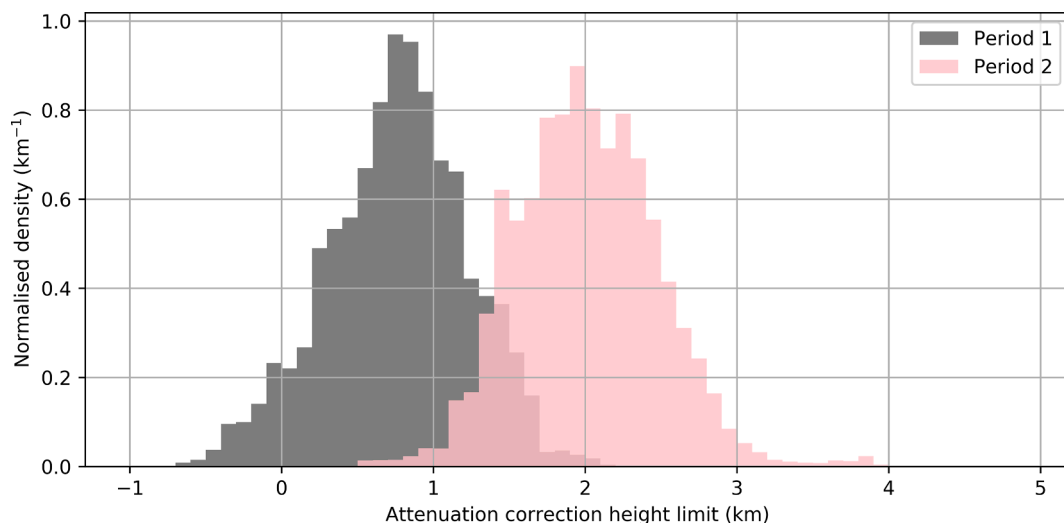

Fig. 6. Distribution of the estimated highest LUE for which the specific attenuation is calculated (250 m below the estimated 0 °C height) for Period 1 (shaded grey) and Period 2 (shaded pink). The distribution was estimated using the air temperature at the NXPol and a lapse rate of 6 °C/km.

R(Dual-Pol) during this period improves its performance, while for R(C-band) many of the catchments suffer from strong positive bias (which actually tends to become increasingly positive for those sites nearest NXPol and correspondingly furthest from the C-band radars) and consequently it suffers a poorer R^2 Efficiency. As assessed by correlation coefficient, the performance of R(Dual-Pol) is only better than that of R(C-band) for 15 of the catchments in the study area. However, this number would be increased to 19 for either R(A_h) or R($A_{h,thr}$). Also recall that NXPol QPEs are experimental prototypes not benefitting from the full complexity of estimation measures featuring in the R(C-band) processing chain. These results are consistent with those presented in Fig. 7 of Neely et al. (2021) comparing R(Dual-Pol) and R(C-band) using the raingauge network data for assessment rather than river flow data.

8. Discussion and concluding remarks

The performance of a set of X-band QPEs produced using data from the NXPol radar - having increasingly complex processing chains and use of dual-polarisation (summarised in Table 1) - were assessed in a hydrological context over northern Scotland. Here, mountainous terrain and low melting layer heights make radar-based QPE challenging. This hydrological assessment used the QPEs as input to a distributed hydrological model, G2G, and compared the resulting set of modelled river flows to observations. The assessment strategy considers how QPEs perform once integrated over space and time, thereby providing additional insights to the meteorological assessment against point raingauge measurements reported by Neely et al. (2021).

All NXPol QPEs assessed showed a clear tendency to underestimate the precipitation for catchments with high mean LUE. The best performance, as assessed by the R^2 Efficiency of the modelled river flows, was generally found for the R(Dual-Pol) and R(KDP-Z) QPEs, while the flows modelled using R(A_h) and R($A_{h,thr}$) QPEs often had the best correlation coefficient. There were clear differences between the two study periods (March to April and June to August 2016) which were caused by the lower melting layer and consequently reduced use of dual-polarisation capability in the first period. A longer study period would allow greater assessment of seasonal effects and reduce the impact of individual weather events.

The strong dependence on LUE of the performance of river flow modelling using NXPol QPEs as input highlights the difficulty of radar precipitation estimation in mountainous environments. Here, the high elevation scans needed to circumvent blockages leads to significant overshooting of the falling precipitation: resulting in low correlation and negative bias of modelled river flows. This effect becomes most apparent when the mean LUE results in utilising radar observations of altitude ~3 km and above. The assessment also highlights that the Met Office C-band radar network suffers from similar issues in this region, but with the results inverted compared to the NXPol radar as a result of the different radar locations. This is despite the more complex processing used in the network radar to attempt to overcome this challenge. Clearly, one solution is to incorporate additional radars into the observing network in these problematic locations, sited such that observations for critical catchments may be made at altitudes less than 3 km. Where this is not feasible, using heavily processed low-elevation scans are likely to be more effective than processed higher-elevation scans. Further improvements to the LUE methodology used herein are required to allow a dynamic use of lower-altitude scan data where possible.

Comparing the assessment results obtained for Period 1 (March to April 2016) with those for Period 2 (July to August 2016), it is seen that the dual-polarisation processing (attenuation correction and specific attenuation based precipitation estimators) has more impact on river flow modelling performance during Period 2. This is a consequence of the requirement to have a continuous path within liquid precipitation to allow more accurate estimation of specific attenuation. Meeting this requirement is often not possible when the freezing height is low and, particularly, when higher elevation-angle scans are needed. Additional processing is required to obtain further benefits (beyond filtering capabilities) from dual-polarisation radars in lower temperature conditions. The expectation is that using solid-phase precipitation estimators based on specific differential phase and reflectivity would improve the results in cold conditions (Bukovčić et al., 2020). Additionally, incorporation of vertical profile corrections and conventional reflectivity estimators better suited to ice-phase hydrometeors may also lead to performance improvements in these conditions. The hydrological simulation approach to assessment used here would be better placed to identify these benefits than a more conventional comparison to data from raingauges as these are less accurate when measuring solid precipitation (Savina et al., 2012). This should be explored in future work.

NXPol QPEs have also been compared to the rain-rate estimates based on observations made by the C-band radar network operated by the UK Met Office. The network radars employ a variety of processing steps not included in the NXPol processing chain. For example, adding an adjustment for mean field bias using raingauge data could be trialled in NXPol. Even so, most NXPol QPEs tended to give higher R^2 Efficiency in modelled river flows than using R(C-band) QPE for catchments near the radar, towards the south-east and the far north of the study area.

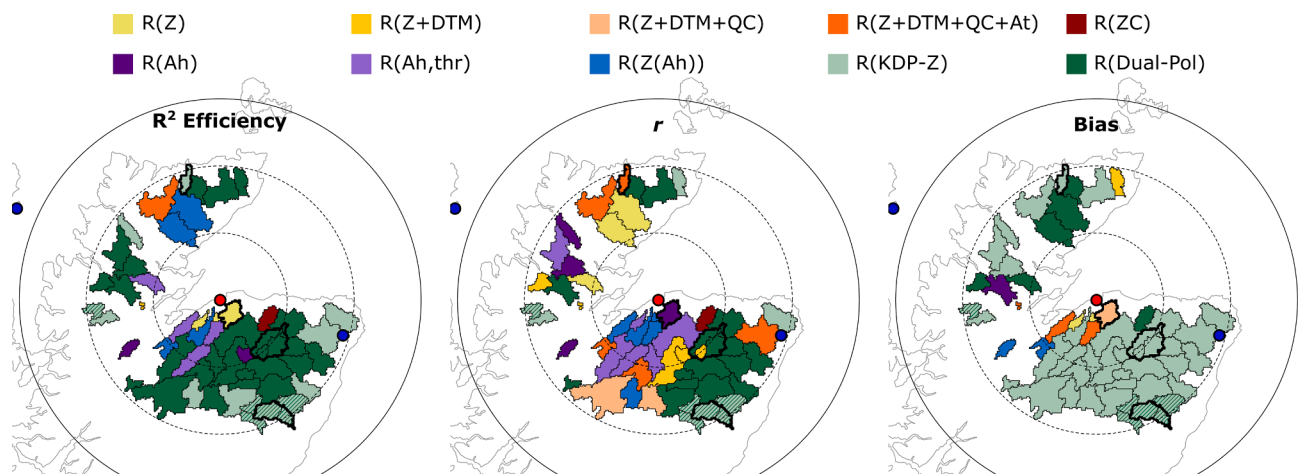The relationship between radar reflectivity and rain-rate used in this

Fig. 7. Catchments are coloured according to the NXPol QPE that produces the best performance in the modelled river flow when assessed using either R^2 Efficiency, correlation or bias. Catchments for which R(Dual-Pol) and R(KDP-Z) perform equally are shown with light-green/dark-green hatching. For bias, the lowest absolute bias is best.
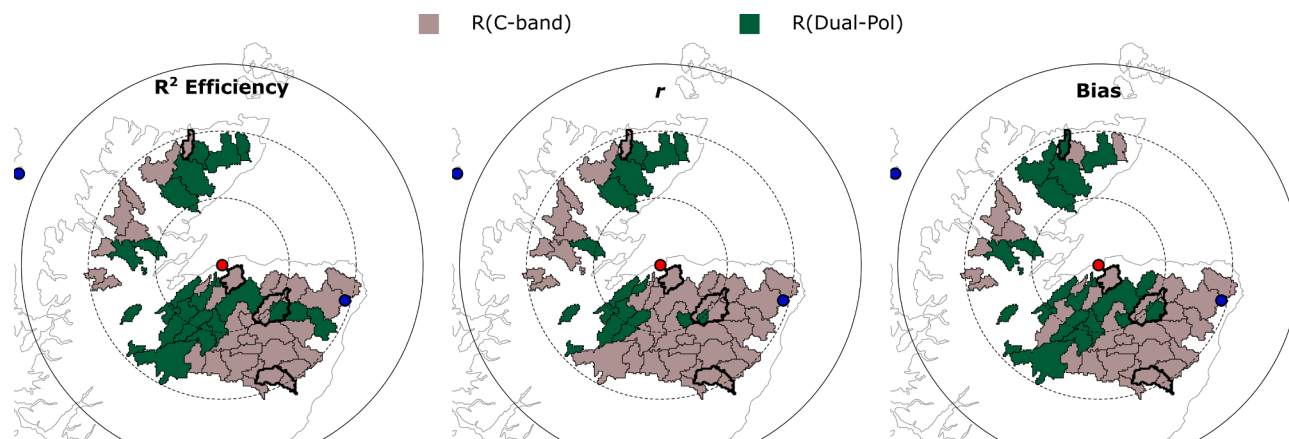
Fig. 8. Catchments are coloured according to whether the R(Dual-Pol) (shaded green) or R(C-band) (shaded grey) QPE produces the best performance in the modelled river flow when assessed using either R^2 Efficiency, correlation or bias. For bias, the lowest absolute bias is best.

study was the Marshall-Palmer relationship (Harrison et al., 2012; Marshall and Palmer, 1948). However, the exact physical relationship between reflectivity and precipitation intensity depends on the drop-size distribution, which in turn depends on type of precipitation, location and season. A preliminary investigation was carried out using data from the Disdrometer Verification Network, DiVeN (Pickering et al., 2019), to measure the drop-size distribution at a location within the coverage of NXPol during the RAiNS campaign (Cairngorm, 2017 to 2019). This suggested that several events were dominated by a large number of smaller drops where the Marshall-Palmer relationship would underestimate rainfall intensity. An initial investigation considering these events, using a bulk average relationship, was tested. It was found to result in large positive biases in modelled river flows for catchments with low LUE, without improving the trend towards negative biases for catchments with high LUE. The conclusion drawn was that a dynamic approach is required, with the Z-R relationship chosen as a function of the observed microphysics, either on a scan-by-scan or voxel-by-voxel basis. Implementation of such a scheme requires further investigation to understand the relationship between drop-size distribution, weather conditions and dual-polarisation radar signatures under UK conditions (Cocks et al., 2019; Thurai et al., 2017).

Further improvements should also consider how the LUE concept introduced in Neely et al. (2021) can be improved upon to preferentially use lower elevation observations where available. This could include using blockage-corrected lower elevations where data exist and higher elevations where there are no echoes available to correct. Also, introducing weighting into the Cartesian gridding scheme to give a higher weight to lower elevation observations within the target grid box where there is a variation in elevations available.

Assessing radar-based QPEs by their effect on modelled river flows (using each QPE as an alternative input to a hydrological model) has been found to be a very useful and independent addition to the assessment against point raingauge measurements performed by Neely et al. (2021). The approach facilitates assessment of precipitation over entire catchment areas, thus circumventing the potential sensitivity to local radar artefacts that can affect raingauge-based assessments, the measurement limitations of raingauges during solid phase precipitation, and also a possible lack of representativity for hard to service locations such as mountain tops. This approach also allows direct assessment of whether the potential benefits of a QPE procedure is carried forward to its quantitative use in hydrological modelling and therefore to end-users. Additionally, the number of suitable catchments in the study area (57) was comparable to the number (64) of raingauges used by Neely et al. (2021). Using a hydrological model to assess QPEs does add complexity and an additional source of uncertainty in the assessment.

However, the accuracy of the QPE appears to be a dominant factor affecting river flow modelling performance. One way to investigate such sensitivity further would be to incorporate an additional hydrological model into the assessment framework, such as a catchment-calibrated lumped rainfall-runoff model. Nevertheless, the hydrological modelling assessment framework presented here has given additional insights into the space–time performance of radar-based QPEs beyond the traditional point-based comparison with raingauge data, and can be easily reapplied to test future QPE developments. Such assessment frameworks have wide applicability and the insights gained - on the performance of dual-polarisation methods and on identifying priority areas for future development - are of general relevance to those developing radar-based QPEs.

CRediT authorship contribution statement

John R. Wallbank: Software, Visualization, Writing – original draft. **David Dufton:** Investigation, Software, Writing – review & editing. **Ryan R. Neely III:** Conceptualization, Resources, Writing – review & editing. **Lindsay Bennett:** Investigation, Software. **Steven J. Cole:** Conceptualization, Methodology, Writing – review & editing. **Robert J. Moore:** Conceptualization, Methodology, Writing – review & editing.

Declaration of Competing Interest

The authors declare that they have no known competing financial interests or personal relationships that could have appeared to influence the work reported in this paper.

Data availability

The NXPol QPEs are from the RAiNS campaign reported by Neely et al. (2021) and the calibrated NXPol radar data are accessible via the CEDA Archive (Bennett, 2019). The R(C-band) QPE data used in this study are identical, up to minor differences due to missing data, to the 1 km resolution UK Composite Rainfall product available from the CEDA Archive (Met Office, 2003).

The river flow and raingauge data were provided by SEPA. For potential evaporation, 40 km gridded monthly values were used - here taken as the monthly average of MORECS PE (Hough and Jones, 1997; Thompson et al., 1981) over the period 1981 to 2010 - available from the UK Met Office. Air temperature data were from the Post Processing of the UK Met Office weather prediction model (UKPP) (Moseley, 2011).

References

Anagnostou, E.N., Anagnostou, M.N., Krakewski, W.F., Kruger, A., Miriovski, B., 2004. High-resolution rainfall estimation from X-band polarimetric radar measurements. J. Hydrometeor. 5, 110–128. https://doi.org/10.1175/1525-7541(2004)005<0110:HREFXP>2.0.CO;2.

Anagnostou, M.N., Nikolopoulos, E.I., Kalogiros, J., Anagnostou, E.N., Marra, F., Mair, E., Bertoldi, G., Tappeiner, U., Borga, M., 2018. Advancing precipitation estimation and streamflow simulations in complex terrain with X-band dual-polarization radar observations. Remote Sensing 10, 1258. https://doi.org/10.3390/rs10081258.

Bell, V.A., Kay, A.L., Jones, R.G., Moore, R.J., Reynard, N.S., 2009. Use of soil data in a grid-based hydrological model to estimate spatial variation in changing flood risk across the UK. J. Hydrol. 377 (3–4), 335–350. https://doi.org/10.1016/j.jhydrol.2009.08.031.

Bennett, L., 2019. RAINS: NCAS mobile X-band radar scan data from Kinloss Barracks, Forres, Scotland, Version 1. Centre for Environmental Data Analysis, 26 February 2019. https://doi.org/10.5285/c86c0daa2e654beda74a79d17624f160.

Berne, A., Krajewski, W.F., 2013. Radar for hydrology: unfulfilled promise or unrecognized potential? Adv. Water Resour. 51, 357–366. https://doi.org/10.1016/j.advwatres.2012.05.005.

Borga, M., Vizzaccaro, A., 1997. On the interpolation of hydrologic variables: formal equivalence of multiquadric surface fitting and kriging. J. Hydrol. 195, 160–171. https://doi.org/10.1016/S0022-1694(96)03250-7.

Bukovčić, P., Rhyzkov, A., Zrnić, D., 2020. Polarimetric relations for snow estimation—radar verification. J. Appl. Meteor. Climatol. 59, 991–1009. https://doi.org/10.1175/JAMC-D-19-0140.1.

Chen, J.-Y., Trömel, S., Ryzhkov, A., Simmer, C., 2021. Assessing the benefits of specific attenuation for quantitative precipitation estimation with a C-band radar network. J. Hydrometeor. 22 (10), 2617–2631. https://doi.org/10.1175/JHM-D-20-0299.1.

Cocks, S.B., Tang, L., Zhang, P., Ryzhkov, A., Kaney, B., Elmore, K.L., Wang, Y., Zhang, J., Howard, K., 2019. A prototype quantitative precipitation estimation algorithm for operational S-band polarimetric radar utilizing specific attenuation and specific differential phase. Part II: Performance verification and case study analysis. J. Hydrometeor. 20 (5), 999–1014. https://doi.org/10.1175/JHM-D-18-0070.1.

Cole, S.J., Moore, R.J., 2008. Hydrological modelling using raingauge- and radar-based estimators of areal rainfall. J. Hydrol. 358, 159–181. https://doi.org/10.1016/j.jhydrol.2008.05.025.

Cole, S.J., Moore, R.J., 2009. Distributed hydrological modelling using weather radar in gauged and ungauged basins. Adv. Water Res. 32 (7), 1107–1120. https://doi.org/10.1016/j.advwatres.2009.01.006.

Cranston, M., Maxey, R., Tavendale, A., Buchanan, P., Motion, A., Cole, S., Robson, A., Moore, R.J., Minett, A., 2012. Countrywide flood forecasting in Scotland: challenges for hydrometeorological model uncertainty and prediction. In: Moore, R.J., Cole, S.J., Illingworth, A.J. (Eds.), Weather Radar and Hydrology (Proc. Exeter Symp., April 2011), IAHS Publ. no. 351, 538–543. https://iahs.info/uploads/dms/15994.096-538-543-351-94-ID166-cranston.pdf.

Darlington, T., Adams, D., Best, S., Husnoo, N., Lyons, S., Norman, K., 2016a. Optimising the accuracy of radar products with dual polarisation: project benefits. Met Office, Exeter, UK, 24pp. https://digital.nmla.metoffice.gov.uk/io_da92368b-0348-4659-82c4-535220600d15/.

Darlington, T., Edwards, M.R.A., Lissaman, V.A., Riley, R., Sugier, J., Kitchen, M., Adams, D., Cox, R., Freeman, N., Norman, K., O'Boyle, R., Sloan, C., Smees, M., 2016b. Designing an operation C-band radar to realise the benefits of dual-polarisation. Met Office Exeter UK 48. https://digital.nmla.metoffice.gov.uk/io_2d8307eb-dfb4-4d6e-8ead-4df70259325e/.

Diederich, M., Ryzhkov, A., Simmer, C., Zhang, P., Trömel, S., 2015a. Use of specific attenuation for rainfall measurement at X-band radar wavelengths. Part I: radar calibration and partial beam blockage estimation. J. Hydrometeor. 16 (2), 487–502. https://doi.org/10.1175/JHM-D-14-0066.1.

Diederich, M., Ryzhkov, A., Simmer, C., Zhang, P., Trömel, S., 2015b. Use of specific attenuation for rainfall measurement at X-band radar wavelengths. Part II: Rainfall estimates and comparison with rain gauges. J. Hydrometeor. 16 (2), 503–516. https://doi.org/10.1175/JHM-D-14-0067.1.

Dufton, D.R.L., 2016. Quantifying Uncertainty In Radar Rainfall Estimates Using an X-Band Dual Polarisation Weather Radar. Ph.D. thesis. University of Leeds, p. 207 pp.. http://etheses.whiterose.ac.uk/15486/.

Dufton, D.R.L., Collier, C.G., 2015. Fuzzy logic filtering of radar reflectivity to remove non-meteorological echoes using dual polarization radar moments. Atmos. Meas. Tech. 8, 3985–4000. https://doi.org/10.5194/amt-8-3985-2015.

Environment Agency, 2007. Rainfall-runoff and other modelling for ungauged/low-benefit locations. Science Report: SC030227/SR1, Authors: R.J. Moore, V.A. Bell, S. J. Cole, D.A. Jones (CEH Wallingford). Research Contractor: CEH Wallingford, Environment Agency, Bristol, UK, 249pp. https://assets.publishing.service.gov.uk/media/602d5aa88fa8f543272b3fa1/_SC030227_tech_report.pdf.

Environment Agency, 2010. Hydrological modelling using convective scale rainfall modelling – phase 3. Project: SC060087/R3, Authors: J. Schellekens, A.R.J. Minett,

P. Reggiani, A.H. Weerts (Deltares); R.J. Moore, S.J. Cole, A.J. Robson, V.A. Bell (CEH Wallingford). Research Contractor: Deltares and CEH Wallingford, Environment Agency, Bristol, UK, 231pp. https://assets.publishing.service.gov.uk/media/602e9bd08fa8f54326ac0bed/Hydrological_modelling_using_convective_scale_rainfall_modelling-_phase_3_technical_report.pdf.

Fabry, F., Bellon, A., Duncan, M.R., Austin, G.L., 1994. High resolution rainfall measurements by radar for very small basins: the sampling problem reexamined. J. Hydrol. 161 (1–4), 415–428. https://doi.org/10.1016/0022-1694(94)90138-4.

Georgiou, S., Gaussiat, N., Lewis, H., 2012. Analysis of a scheme to dynamically model the orographic enhancement of precipitation in the UK. In: Moore, R.J., Cole, S.J., Illingworth, A.J. (Eds.), Weather Radar and Hydrology (Proc. Exeter Symp., April 2011), IAHS Publ. no. 351, 201–206. https://iahs.info/uploads/dms/15890.038-201-206-351-02-ID-010.pdf.

Gourley, J.J., Giangrande, S.E., Hong, Y., Flamig, Z.L., Schuur, T., Vrugt, J.A., 2010. Impacts of polarimetric radar observations on hydrologic simulation. J. Hydrometeor. 11, 781–796. https://doi.org/10.1175/2010JHM1218.1.

Gupta, H.V., Kling, H., Yilmaz, K.K., Martinez, G.F., 2009. Decomposition of the mean squared error and NSE performance criteria: Implications for improving hydrological modelling. J. Hydrol. 377, 80–91. https://doi.org/10.1016/j.jhydrol.2009.08.003.

Hardy, R.L., 1971. Multiquadric equations of topography and other irregular surfaces. J. Geophys. Res. 76 (8), 1905–1915. https://doi.org/10.1029/JB076i008p01905.

Harrison, D.L., Driscoll, S.J., Kitchen, M., 2006. Improving precipitation estimates from weather radar using quality control and correction techniques. Meteorol. Appl. 7 (2), 135–144. https://doi.org/10.1017/S1350482700001468.

Harrison, D.L., Scovell, R.W., Kitchen, M., 2009. High-resolution precipitation estimates for hydrological uses. Water Manage. 162, 125–135. https://doi.org/10.1680/wama.2009.162.2.125.

Harrison, D.L., Norman, K., Pierce, C., Gaussiat, N., 2012. Radar products for hydrological applications in the UK. Water Manage. 165, 89–103. https://doi.org/10.1680/wama.2012.165.2.89.

He, X., Koch, J., Zheng, C., Bøvith, T., Jensen, K.H., 2018. Comparison of simulated spatial patterns using rain gauge and polarimetric-radar-based precipitation data in catchment hydrological modeling. J. Hydrometeor. 19, 1273–1288. https://doi.org/10.1175/JHM-D-17-0235.1.

Heistermann, M., Jacobi, S., Pfaff, T., 2013. Technical Note: An open source library for processing weather radar data (wradlib). Hydrol. Earth Syst. Sci. 17, 863–871. https://doi.org/10.5194/hess-17-863-2013.

Helmus, J., Collis, S., 2016. The Python ARM Radar Toolkit (Py-ART), a library for working with weather radar data in the Python programming language. J. Open Res. Software 4 (1), e25. https://doi.org/10.5334/jors.119.

Hough, M.N., Jones, R.J.A., 1997. The United Kingdom Meteorological Office Rainfall and Evaporation Calculation System: MORECS version 2.0 – an overview. Hydrol. Earth Syst. Sci. 1, 227–239. https://doi.org/10.5194/hess-1-227-1997.

Howard, P.J., Cole, S.J., Robson, A.J., Moore. R.J., 2012. Raingauge quality-control algorithms and the potential benefits for radar-based hydrological modelling. In: Moore, R.J., Cole, S.J., Illingworth, A.J. (Eds.), Weather Radar and Hydrology (Proc. Exeter Symp., April 2011), IAHS Publ. no. 351, 219–-224. https://iahs.info/uploads/dms/15894.041-219-224-351-40-ID-167-Howard-et-al.pdf.

Hubbert, J., Bringi, V.N., 1995. An iterative filtering technique for the analysis of copolar differential phase and dual-frequency radar measurements. J. Atmos. Oceanic Technol. 12 (3), 643–648. https://doi.org/10.1175/1520-0426(1995)012<0643:AIFTFT>2.0.CO;2.

Illingworth, A.J., 2004. Improved precipitation rates and data quality by using polarimetric measurements. In: Meischner, P. (Ed.), Weather Radar. Physics of Earth and Space Environments. Springer, pp. 130–166.

Kling, H., Fuchs, M., Paulin, M., 2012. Runoff conditions in the upper Danube basin under an ensemble of climate change scenarios. J. Hydrol. 424–425, 264–277. https://doi.org/10.1016/j.jhydrol.2012.01.011.

Koistinen, J., Pohjola, H., 2014. Estimation of ground-level reflectivity factor in operational weather radar networks using VPR-based correction ensembles. J. Appl. Meteor. Climatol. 53, 2394–2411. https://doi.org/10.1175/JAMC-D-13-0343.1.

Lim, S., Lee, D.-R., Cifelli, R., Hwang, S.H., 2014. Quantitative precipitation estimation for an X-band dual-polarization radar in the complex mountainous terrain. KSCE J. Civ. Eng. 18, 1548–1553. https://doi.org/10.1007/s12205-014-0439-9.

Marshall, J.S., Palmer, W., 1948. The distribution of raindrops with size. J. Meteorol. 5, 165–166. https://doi.org/10.1175/1520-0469(1948)005<0165:TDORWS>2.0.CO;2.

Met Office, 2003. 1 km Resolution UK Composite Rainfall Data from the Met Office Nimrod System. NCAS British Atmospheric Data Centre. https://catalogue.ceda.ac.uk/uuid/27dd6ffba67f667a18c62de5c3456350.

Met Office, 2018. UK climate averages. Met Office accessed 17 June 2021. https://www.metoffice.gov.uk/research/climate/maps-and-data/uk-climate-averages.

Met Office, 2020. Factsheet 15 – Weather radar. National Meteorological Library and Archive, Met Office, Exeter, UK, 24pp. https://www.metoffice.gov.uk/research/library-and-archive/publications/factsheets.

Montopoli, M., Roberto, N., Adirosi, E., Gorgucci, E., Baldini, L., 2017. Investigation of weather radar quantitative precipitation estimation methodologies in complex orography. Atmosphere 8 (2), 34. https://doi.org/10.3390/atmos8020034.

Moore, R.J., 1985. The probability-distributed principle and runoff production at point and basin scales. Hydrol. Sci. J. 30 (2), 273–297. https://doi.org/10.1080/02626668509490989.

Moore, R.J., 2007. The PDM rainfall-runoff model. Hydrol. Earth Syst. Sci. 11, 483–499. https://doi.org/10.5194/hess-11-483-2007.

Moore, R.J., Bell, V.A., Austin, R.M., Harding, R.J., 1999. Methods for snowmelt forecasting in upland Britain. Hydrol. Earth Syst. Sci. 3, 233–246. https://doi.org/10.5194/hess-3-233-1999.

Moore, R.J., Cole, S.J., Bell, V.A., Jones, D.A., 2006. Issues in flood forecasting: Ungauged basins, extreme floods and uncertainty. In: I. Tchiguirinskaia, K.N.N. Thein & P. Hubert (Eds.), Frontiers in Flood Research, 8th Kovacs Colloquium, UNESCO, Paris, June/July 2006, IAHS Publ. 305, 103–122. https://iahs.info/uploads/dms/13517.09-103-122-305-07-Moore-et-al.pdf.

Moore. R.J., Cole, S.J., Robson, A.J., 2012. Weather radar and hydrology: a UK operational perspective. In: Moore, R.J., Cole, S.J., Illingworth, A.J. (Eds.), Weather Radar and Hydrology (Proc. Exeter Symp., April 2011), IAHS Publ. no. 351, 429–434. https://iahs.info/uploads/dms/15976.078-429-434-ID-177–Moore-et-al–Keynote-v3.pdf.

Moseley, S., 2011. From observations to forecasts - Part 12: Getting the most out of model data. Weather 66 (10), 272–276. https://doi.org/10.1002/wea.844.

Nash, J.E., Sutcliffe, J.V., 1970. River flow forecasting through conceptual models Part I – a discussion of principles. J. Hydrol. 10, 282–290. https://doi.org/10.1016/0022-1694(70)90255-6.

Neely III, R., Bennett, L., Blyth, A., Collier, C., Dufton, D., Groves, J., Walker, D., Walden, C., Bradford, J., Brooks, B., Addison, F.I., Nicol, J., Pickering, B., 2018. The NCAS mobile dual-polarisation Doppler X-band weather radar (NXPol). Atmos. Meas. Tech. 11, 6481–6494. https://doi.org/10.5194/amt-11-6481-2018.

Neely III, R.R., Parry, L., Dufton, D., Bennett, L., Collier, C., 2021. Radar applications in Northern Scotland (RAiNS). J. Hydrometeor. 22 (2), 483–498. https://doi.org/10.1175/JHM-D-19-0184.1.

Pickering, B.S., Neely III, R.R., Harrison, D., 2019. The disdrometer verification network (DiVeN): a UK network of laser precipitation instruments. Atmos. Meas. Tech. 12, 5845–5861. https://doi.org/10.5194/amt-12-5845-2019.

Price, D., 1999. Systematic error of standard UK raingauges in the central Scottish Highlands. Weather 54 (10), 334–341. https://doi.org/10.1002/j.1477-8696.1999.tb03994.x.

Price, D., Hudson, K., Boyce, G., Schellekens, J., Moore, R.J., Clark, P., Harrison, T., Connolly, E., Pilling, C., 2012. Operational use of a grid-based model for flood forecasting. Water Manage. 165 (2), 65–77. https://doi.org/10.1680/wama.2012.165.2.65.

Ryzhkov, A.V., Zrnić, D.S., 2019. Polarimetric measurements of precipitation. In: Ryzhkov, A.V., Zrnić, D.S. (Eds.), Radar Polarimetry for Weather Observations. Springer, pp. 373–433. https://doi.org/10.1007/978-3-030-05093-1_10.

Ryzhkov, A., Diederich, M., Zhang, P.F., Simmer, C., 2014. Potential utilization of specific attenuation for rainfall estimation, mitigation of partial beam blockage, and radar networking. J. Atmos. Oceanic Technol. 31 (3), 599–619. https://doi.org/10.1175/JTECH-D-13-00038.1.

Ryzhkov, A.V., Zrnić, D.S., 1995. Comparison of dual-polarization radar estimators of rain. J. Atmos. Oceanic Technol. 12 (2), 249–256. https://doi.org/10.1175/1520-0426(1995)012<0249:CODPRE>2.0.CO;2.

Sachidananda, M., Zrnić, D.S., 1986. Differential propagation phase shift and rainfall rate estimation. Radio Science 21 (2), 235–247. https://doi.org/10.1029/RS021i002p00235.

Savina, M., Schäppi, B., Molnar, P., Burlando, P., Sevruk, B., 2012. Comparison of a tipping-bucket and electronic weighing precipitation gage for snowfall. Atmos. Res. 103, 45–51. https://doi.org/10.1016/j.atmosres.2011.06.010.

Sevruk, B., 1982. Methods of correction for systematic error in point precipitation measurement for operational use. WMO Operational Hydrology Report No. 21, 91pp. https://library.wmo.int/doc_num.php?explnum_id=1238.

Testud, J., Le Bouar, E., Obligis, E., Ali-Mehenni, M., 2000. The rain profiling algorithm applied to polarimetric weather radar. J. Atmos. Oceanic Technol. 17, 332–356. https://doi.org/10.1175/1520-0426(2000)017<0332:TRPAAT>2.0.CO;2.

Thompson, N., Barrie, I.A., Ayles, M., 1981. The Meteorological Office Rainfall and Evaporation Calculation System: MORECS (July 1981). Hydrological Memorandum No. 45, Meteorological Office.

Thorndahl, S., Einfalt, T., Willems, P., Nielsen, J.E., ten Veldhuis, M.-C., Arnbjerg-Nielsen, K., Rasmussen, M.R., Molnar, P., 2017. Weather radar rainfall data in urban hydrology. Hydrol. Earth Syst. Sci. 21, 1359–1380. https://doi.org/10.5194/hess-21-1359-2017.

Thurai, M., Mishra, K.V., Bringi, V.N., Krajewski, W.F., 2017. Initial results of a new composite-weighted algorithm for dual-polarized X-band rainfall estimation. J. Hydrometeor. 18 (4), 1081–1100. https://doi.org/10.1175/JHM-D-16-0196.1.

Vulpiani, G., Montopoli, M., Passeri, L.D., Gioia, A.G., Giordano, P., Marzano, F.S., 2012. On the use of dual-polarized C-band radar for operational rainfall retrieval in mountainous areas. J. Appl. Meteor. Climatol. 51, 405–425. https://doi.org/10.1175/JAMC-D-10-05024.1.

Wijayarathne, D., Boodoo, S., Coulibaly, P., Sills, D., 2020. Evaluation of radar Quantitative Precipitation Estimates (QPEs) as an input of hydrological models for hydrometeorological applications. J. Hydrometeor. 21 (8), 1847–1864. https://doi.org/10.1175/JHM-D-20-0033.1.

Worsfold, M., Norman, K., Harrison, D., 2014. Analysis of Weather Radar Coverage Over Scotland Using A High Density Tipping Bucket Rain-Gauge Network. Met Office, Exeter, UK, p. 41.

Yu, N., Gaussiat, N., Tabary, P., 2018. Polarimetric X-band weather radars for quantitative precipitation estimation in mountainous regions. Q. J. R. Meteorol. Soc. 144, 2603–2619. https://doi.org/10.1002/qj.3366.